Hybrid Advances 2 (2023) 100024

Contents lists available at ScienceDirect

Hybrid Advances

journal homepage: www.journals.elsevier.com/hybrid-advances

Ultrasonic pulse velocity and physical properties of hybrid composites: A statistical approach

Sergio Luiz Moni Ribeiro Filho [a], Carlos Thomas [b], Luís Miguel Pereira Durão [c], André Luis Christoforo [d], Chris Bowen [e], Fabrizio Scarpa [f], Tulio Hallak Panzera [a,*]

[a] Centre for Innovation and Technology in Composite Materials – CIT^{e}C, Department of Mechanical Engineering, Federal University of São João del Rei (UFSJ), Brazil
[b] LADICIM (Laboratory of Materials Science and Engineering), Universidad de Cantabria, Spain
[c] ISEP/CIDEM, Instituto Superior de Engenharia do Porto, Centro de Investigação e Desenvolvimento em Engenharia Mecânica, Portugal
[d] Department of Civil Engineering, Federal University of São Carlos (UFSCar), Brazil
[e] Department of Mechanical Engineering, University of Bath, UK
[f] Bristol Composites Institute, University of Bristol, UK

A B S T R A C T

This work describes the correlations between the ultrasonic pulse velocity (UPV) and physical properties of fibrous-particulate hybrid composites made of glass/carbon fabrics and three different micro-inclusions such as silica particles, recycled carbon fibre powder and Portland cement. A full factorial design ($2^1 4^1 5^1$) is established to identify the effects of volume fraction, stacking sequence and particle type on the physical properties obtained by Archimedes' principle. An electroacoustic transducer (50 kHz) is used to determine the ultrasonic pulse velocity data. Statistical models reveal correlations between UPV and the physical properties of hybrid composites. The combination of UPV and statistical techniques can identify all constitutive phases, being useful to characterise and estimate physical properties in a hybrid system composed of fibres and microparticles.

1. Introduction

Non-destructive testing (NDT) has, for some time, become essential for affordable integrity control and strength assessment for concrete structures, but also hybrid composites [1,2]. Among these NDT methods, the ultrasonic pulse velocity-based propagation system (UPV) is the most widely and successfully used because of its accessible, direct, reliable and inexpensive features [3].

UPV wave characteristics, such as amplitude, velocity, attenuation, frequency and energy, play an important role in estimating the strength and evaluating damages and defects of composite structures. The most significant feature of UPV techniques is their ability to indirectly correlate and connect to the physical and mechanical properties of cementitious and polymeric composites [4–7]. Some works in the open literature have developed theoretical models and correlations to predict the strength/physical properties of cement products via UPV analysis. Panzera et al. [4] found a linear response correlation between UPV and compressive strength, bulk density, apparent porosity, oxygen permeability and modulus of elasticity for a compacted Portland silica-cement set. Nascimento et al. [5] conducted experiments to establish correlation models to predict the physical and mechanical properties of mortars containing polypropylene (PP) aggregates. Lin et al. [6] investigated the effect of the aggregate content and the water-cement ratio of concrete on predicting models via UPV. Trtnik et al. [7] reported that aggregate characteristics such as size, amount, type and shape are very important in assessing the compressive strength of the mineral-admixture concrete through UPV measurements. In addition, recent publications have addressed the use of the UPV method not only for strength prediction, but also for monitoring concrete hydration. Zhang et al. [8] found patterns related to cement hydration stages based on ultrasonic pulse waves. Three stages were observed: constant regime, in which the waves propagate through a viscous interface (liquid phase), fast growth regime related to the beginning of hydrated products and slow growth regime when the solid phase of the aggregates and cement mixture is connected. A similar feature was reported by Trtnik et al. [9] and Ye et al. [10].

Ultrasonic pulse waves can be considered the most reliable method for evaluating the overall integrity and failure of the material, as well as determining its elastic properties [3]. Regarding orthotropic materials, the determination of wave velocity and elastic properties is somewhat complicated by the small thickness of the laminated components [11,12]. Böhm and Hufenbach [13] stated that the typical small thickness combined with the requirement of the incident angle in laminated composites

* Corresponding author.
E-mail address: panzera@ufsj.edu.br (T.H. Panzera).

https://doi.org/10.1016/j.hybadv.2023.100024
Received 6 December 2022; Received in revised form 23 January 2023; Accepted 24 January 2023
Available online 25 January 2023

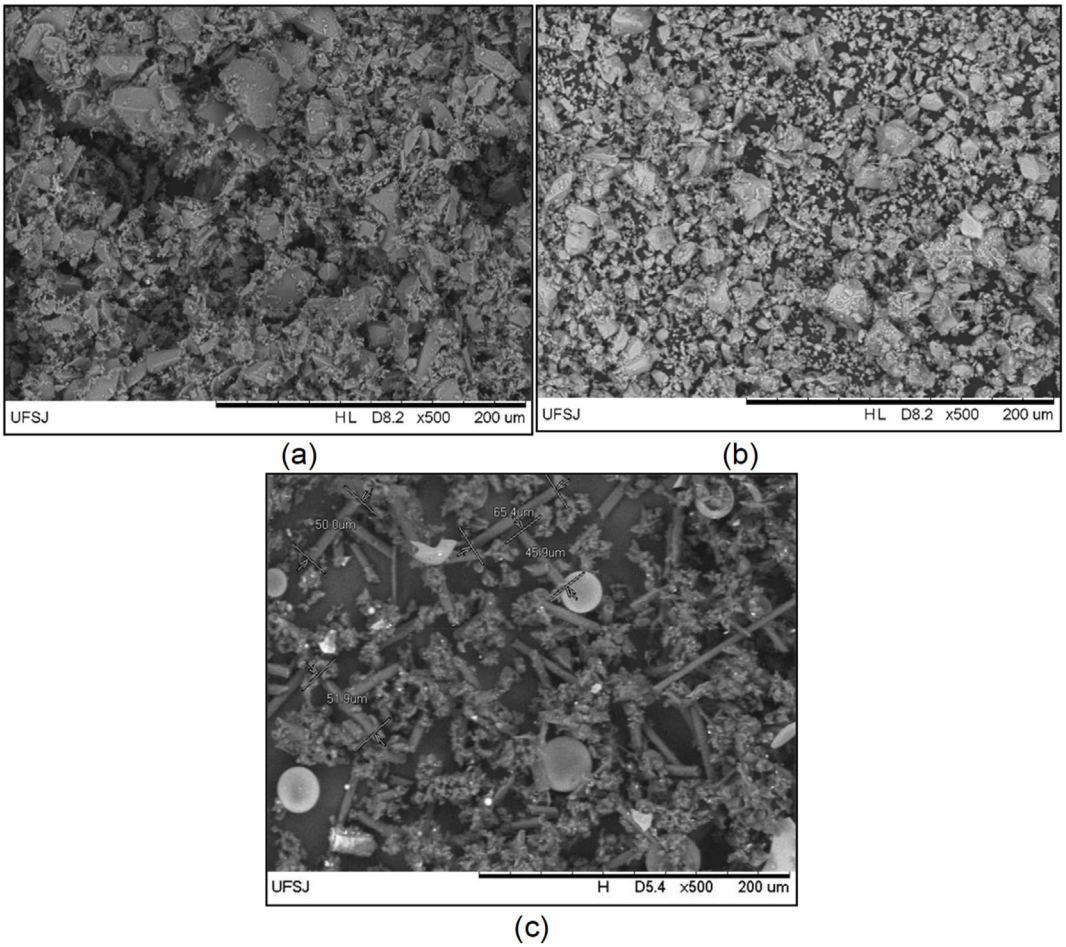

Fig. 1. Scanning electron microscopy of (a) silica, (b) cement and (c) carbon microfibre wastes.

does not allow the propagation of the transverse wave in the symmetrical plane. Alternatively, Hufenbach et al. [14] and, Adoin and Baste [15] suggested performing a set of velocity measurements in a non-symmetry plane. Hufenbach et al. [14] developed a specific ultrasonic device to measure the anisotropic damage of fibres and textile-reinforced composites. Adoin and Baste [15] showed that it is possible to measure the stiffness tensor of an anisotropic material through an ultrasonic technique. Castellano et al. [16] proposed a non-destructive experimental approach to determine five elastic moduli of CFRP by the ultrasonic immersion test. The authors demonstrated a deeper insight into the ultrasonic wave propagation phenomena and determined the phase velocities and phase angles of the anisotropic material. Chang et al. [17] evaluated the influence of fibre/matrix interface shape, volume fraction, and fibre arrangements on the propagation of ultrasonic waves in glass fibre-reinforced polymer (FRP). Numerical simulations showed that the interface between the fibre and the matrix substantially altered the wave motion. One part of the wave was reflected and scattered around the fibre, and the other was transmitted and propagated in the polymer matrix. Sokolovskaya et al. [18] performed experiments to measure the CFRP attenuation coefficient and phase velocity. The authors reported that the porosity level was strongly correlated with the ultrasonic velocity wave, i.e., increased porosity leads to reduced UPV values. Zelenyak et al. [19] modelled the interaction of the ultrasonic wave field in FRPs with defects, such as delamination and cracking. Ultrasonic inspection using the 3D-FEM model described the interaction of defective ultrasonic waves, providing a useful tool to predict the propagation waves in some complex damage zones.

Hybrid composites can be considered highly complex and heterogeneous. This complexity makes the UPV inspection extremely limited, where only visible macroscopic and microscopic damage is accessible, and no quantitative information is obtained [17]. This research is inspired by the fact that no comprehensive study has been performed regarding the possible use of longitudinal pulse velocity in evaluating the physical properties of hybrid laminate composites composed of microparticles (silica, Portland cement and carbon microfibres wastes) and two different fibres (glass and carbon). The effects of fibre volume fraction, fibre stacking sequence and particle type factors on apparent porosity, water absorption, density and UPV responses are investigated using a statistical full factorial design. Finally, analytical relationships between the physical properties and ultrasonic pulse velocity are proposed.

2. Materials and method

2.1. Raw materials

The hybrid composites are composed of an epoxy matrix and dispersive phases consisting of microparticles (cement, silica, recycled carbon microfibres – CMF) and carbon/glass fibres. Renlam M epoxy resin and catalyst agent HY 956 are supplied by Huntsman (Brazil). Cross-ply carbon and glass fabrics (200 g/m^2) are provided by *Texiglass (Brazil)*. Silica, Portland cement (ASTM Type III, supplied by Holcim-Brazil) and CMF aggregates are individually added to the matrix phase as an additional mechanism to enhance the matrix stiffness and increase the interlaminar shear locking effect. Silica and cement particles are classified by sieving in a monomodal particle size distribution (325–400 US-Tyler). CMF wastes are microfibres obtained from the CFRP-cutting process. Silica and CMF are considered non-reactive, while cement is

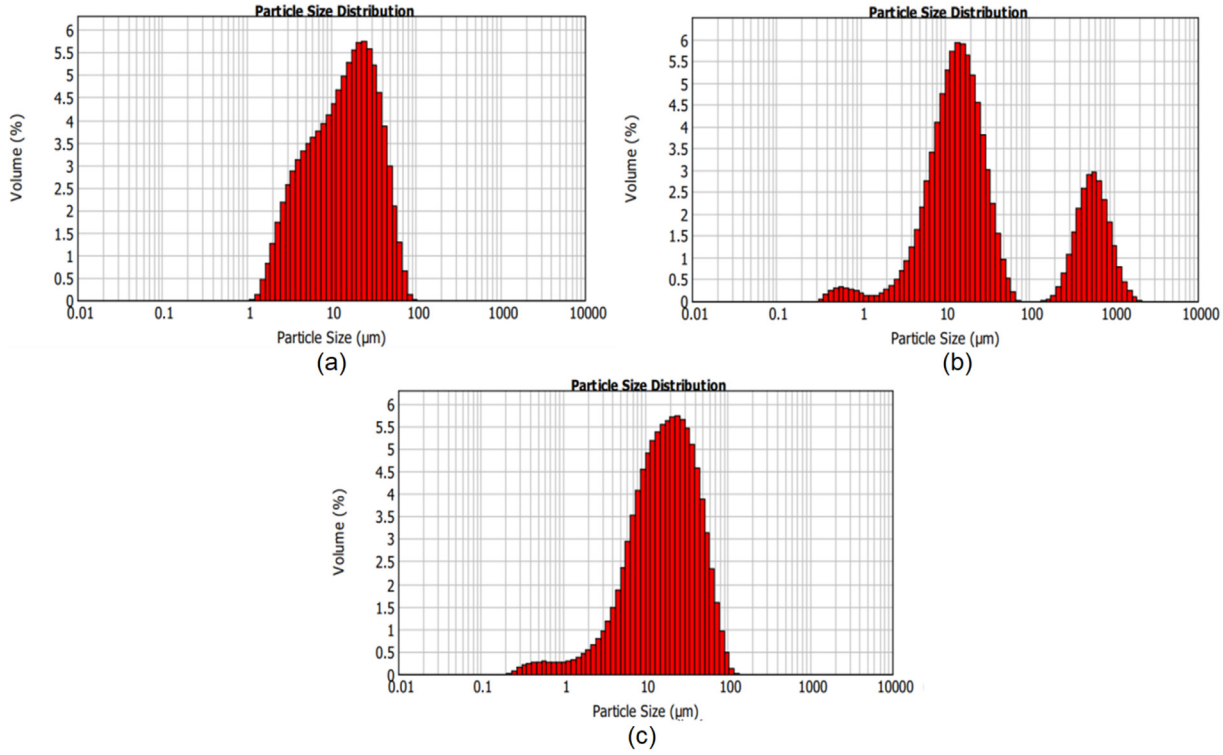

Fig. 2. Particle size distribution curves of: (a) silica, (b) cement and (c) carbon microfibres.

potentially reactive due to the presence of epoxy polymerisation; such effect is still discussed in the literature [20,21].

Fig. 1 shows the microstructural analysis of the particles obtained by the Hitachi (TM-3000) scanning electron microscope. The silica (Fig. 1a) and cement (Fig. 1b) particles are classified as tetrahedral (angular) due to the grinding of quartz ore and clinker, respectively. CMF wastes are cylindrical microfibres obtained from the CFRP cutting process (Fig. 1c). Its high aspect ratio can affect the results obtained by the laser diffraction technique. The spheres shown in the image (Fig. 1c) are metallic oxides used as pigments during the manufacturing of fins.

A particle size analysis is performed by laser diffraction on the Martersizer 2000 device. Fig. 2a shows the distribution of silica particles with sizes ranging from 2 to 70 μm. Cement particles (Fig. 2b) have three average sizes, a small amount smaller than 1 μm, a large amount between 3 and 50 μm, and a medium portion between 300 and 1000 μm. This distribution suggests that other materials, comminute separately, are added to the cement. A small amount of the CMF particles is noticed below 1 μm, with the majority between the range of 15 and 40 μm (Fig. 2c).

2.2. Manufacturing

Fibrous-particulate reinforced polymers are manufactured using a hand lay-up method at room-temperature (28±1 °C, RH 52 ± 1%). The epoxy resin is oven-heated at 50 °C to eliminate air bubbles and reduce viscosity to facilitate the dispersion of particles. The silica, cement and CMF are mixed with the epoxy resin for 5 min and then spread over the glass/carbon fabrics. Five-layer architectures with different stacking sequences and fibre volume fractions (40/60 and 60/40) are considered. The variation of the stacking sequences is defined to evaluate the asymmetry/symmetry of the hybrid laminates. Preliminary tests are conducted to determine the optimal particle fraction (9 wt%) based on the mechanical stiffness of the particulate-reinforced polymers. The particle weight fraction (9 wt%) is calculated based on the fibre/matrix volume phase to maintain the same nominal particle distribution. Gas pycnometer tests (Micromeritics model AccuPyc 1330) are performed on

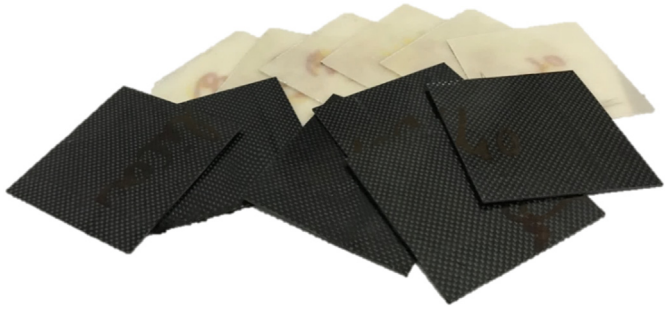

Fig. 3. Hybrid laminates samples.

Portland cement and silica to determine their apparent density. The composites are compacted in a vacuum chamber applying a pressure of 0.8 bar, and then cured at room temperature (24 °C) for 28 days. The plates are cut to sample sizes of 100 × 100 mm^2, as shown in Fig. 3.

2.3. Physical properties

Based on the Archimedes principle, apparent density is determined following the ASTM D792 protocol [22], using a vacuum saturation method with distilled water at 19 °C and a precision scale of 0.0001 g. The apparent density (ρ_a) can be calculated as:

$$\rho_a = \frac{W_1}{Vi} \tag{1}$$

In Equation (1), ρ_a is the apparent density (kg/m^3), W_1 is the dry mass of the laminate (kg), and V_i is the impervious volume of the laminate (m^3). Volume V_i can be determined by considering the water density of 1000 kg/m^3:

$$V_i = \frac{W_1 - W_3}{1000} \tag{2}$$

In Equation (2), W_3 is the mass of the laminate fully submerged in water (kg).

Apparent porosity is the ratio between the volume of open pores and the external volume of the impermeable portion of the sample. The apparent porosity (P_a) is obtained by the Archimedes principle, using the vacuum saturation method based on ASTM C1039-85 [24]. Equation (3) establishes the apparent porosity as a function of the dry mass (W_1), saturated mass (W_2) and submerged mass (W_3) of the laminate:

$$Pa = \frac{W_2 - W_1}{W_2 - W_3} \times 100 \tag{3}$$

The water absorption A_b is obtained from the percentage of water absorbed by the specimen after submersion in water under constant negative pressure, following the recommendations of ASTM C1039-85 [23]:

$$A_b = \frac{W_2 - W_1}{W_1} \times 100 \tag{4}$$

2.4. Ultrasonic pulse velocity

The hybrid specimens in this work are an orthotropic material, being stiff along the fibre direction but compliant along the orthogonal directions. As 1.5 mm thick quadratic samples are used, measurements in plane 1–3 are not possible. However, due to its symmetrical cross-ply structure, the hybrid laminate possesses two other perpendicular planes of symmetry. It satisfies the hypothesis of an orthorhombic system required by the ultrasonic technique [11–15]. As a result, the ultrasonic pulse waves are obtained by an electroacoustic transducer (50 kHz) coupled to the portable digital tester (Pundit Plus). The transducers are located on opposite sides of the specimen, with direct transmission. Silicone grease is used as a coupling agent between the transducer and laminate surfaces to maximise the accuracy of signal measurements and ensure no air gap. Longitudinal vibration is measured by the specifications of British Standard 1881:203 [25]. The ultrasonic pulse velocity is directly related to the stress wave propagation based on the measurement of transit time (T) and wave path length (L) of the laminates. Thus, the velocity ($m.s^{-1}$) is given by:

$$\vartheta = \frac{L}{T} \tag{5}$$

2.5. Experimental design

Design of Experiment (DoE) is a methodology that uses different statistical techniques to provide a structured planning method, executing and analysing experiments [26]. DoE is also essential to identify which factors and parameters are most significant for the overall properties of composites [26,27]. ANOVA (analysis of variance) is used to verify if the effect of the main factors and the interaction of the factors are statistically significant. Interaction effects occur when the effect of one variable depends on another variable [26]. A P-value less than or equal to 0.05 (α-level of 0.05) indicates a significant effect within a 95% confidence interval. The Anderson-Darling normality test is also performed to examine and identify whether the residuals of the response variables follow a normal distribution. When the P-value for the Anderson-Darling test is greater than 0.05 (i.e., an α-level of 0.05), the data follow a normal distribution, thus validating the results of the ANOVA model [26]. In addition, Tukey's multiple comparison analysis is used to compare the experimental levels as a treatment grouping. Tukey's test results are illustrated in the main effect plots only. Figs. 4–5, 8 and 9 exhibit the results of the grouping obtained by Tukey's tests, in which statistically equivalent means are represented by equal letters. The groups with the highest means are denoted by A, followed by B, C, and so on, as the means decrease. Each sample is manufactured individually, which corresponds to a replicate. Four replicates are considered for each of the 48 experimental conditions. A replicate consists of repeating the experimental condition so that the error associated with the individual response can be estimated. The magnitude of this error is important to identify significant effects attributed to factor selection. A randomization procedure is also adopted during the experimental tests, making the entire numerical process more robust against uncontrollable or unknown variables in the experiment, which can impact the response.

A $2^1 4^1 5^1$ full factorial design is performed to investigate the effect of stacking sequence, volume fraction and particle type on ultra-pulse velocity and physical responses of hybrid composites. Tables 1 and 2 show the factors and experimental levels used in the statistical design. ANOVA and DoE are performed using Minitab® and R® statistical softwares.

Table 1
Matrix planning.

Factors	Experimental levels
Stacking Sequence	Only Glass Fibres (G_5)
	Only Carbon Fibres (C_5)
	Glass/Glass/Glass/Carbon/Carbon (G_3C_2)
	Carbon/Glass/Glass/Glass/Carbon (CG_3C)
	Glass/Carbon/Glass/Carbon/Glass (GCGCG)
Volume Fraction [wt%]	40/60
	60/40
Type of particle	No particle
	Silica
	Cement
	CMF

Table 2
Experimental conditions.

Condition	Volume Fraction [%]	Type of Particle	Stacking Sequence
C1	40/60	No particle	G_5
C2	40/60	No particle	C_5
C3	40/60	No particle	G_3C_2
C4	40/60	No particle	GCGCG
C5	40/60	No particle	CG_3C
C6	40/60	Silica	G_5
C7	40/60	Silica	C_5
C8	40/60	Silica	G_3C_2
C9	40/60	Silica	GCGCG
C10	40/60	Silica	CG_3C
C11	40/60	Cement	G_5
C12	40/60	Cement	C_5
C13	40/60	Cement	G_3C_2
C14	40/60	Cement	GCGCG
C15	40/60	Cement	CG_3C
C16	40/60	CMF	G_5
C17	40/60	CMF	C_5
C18	40/60	CMF	G_3C_2
C19	40/60	CMF	GCGCG
C20	40/60	CMF	CG_3C
C21	60/40	No particle	G_5
C22	60/40	No particle	C_5
C23	60/40	No particle	G_3C_2
C24	60/40	No particle	GCGCG
C25	60/40	No particle	CG_3C
C26	60/40	Silica	G_5
C27	60/40	Silica	C_5
C28	60/40	Silica	G_3C_2
C29	60/40	Silica	GCGCG
C30	60/40	Silica	CG_3C
C31	60/40	Cement	G_5
C32	60/40	Cement	C_5
C33	60/40	Cement	G_3C_2
C34	60/40	Cement	GCGCG
C35	60/40	Cement	CG_3C
C36	60/40	CMF	G_5
C37	60/40	CMF	C_5
C38	60/40	CMF	G_3C_2
C39	60/40	CMF	GCGCG
C40	60/40	CMF	CG_3C

Table 3
ANOVA results for apparent porosity, water absorption and apparent density.

Main factor and interactions	Full factorial design $2^1 4^1 5^1 = 40$					
	Apparent Porosity [%]		Water Absorption [%]		Apparent density [g/m^3]	
	Contribution	P-value ≤ 0.05	Contribution	P-value ≤ 0.05	Contribution	P-value ≤ 0.05
Volume Fraction	54.96%	0.000	51.46%	0.000	5.97%	0.000
Particle Type	13.68%	0.000	16.76%	0.000	4.02%	0.000
Stacking Sequence	3.74%	0.000	3.10%	0.000	50.47%	0.000
Fraction*Particle type	3.02%	0.000	5.93%	0.000	2.81%	0.003
Fraction*Stacking	3.03%	0.000	2.37%	0.000	20.12%	0.000
Particle Type*Stacking	14.17%	0.000	11.95%	0.000	5.17%	0.015
Fraction*Particle Type*Stacking	7.08%	0.000	8.23%	0.000	4.57%	0.029
R^2 (adj)	99.37%		99.58%		99.05%	
Anderson-Darling test	P-value = 0.296 ≥ 0.05		P-value = 0.102 ≥ 0.05		P-value = 0.261 ≥ 0.05	

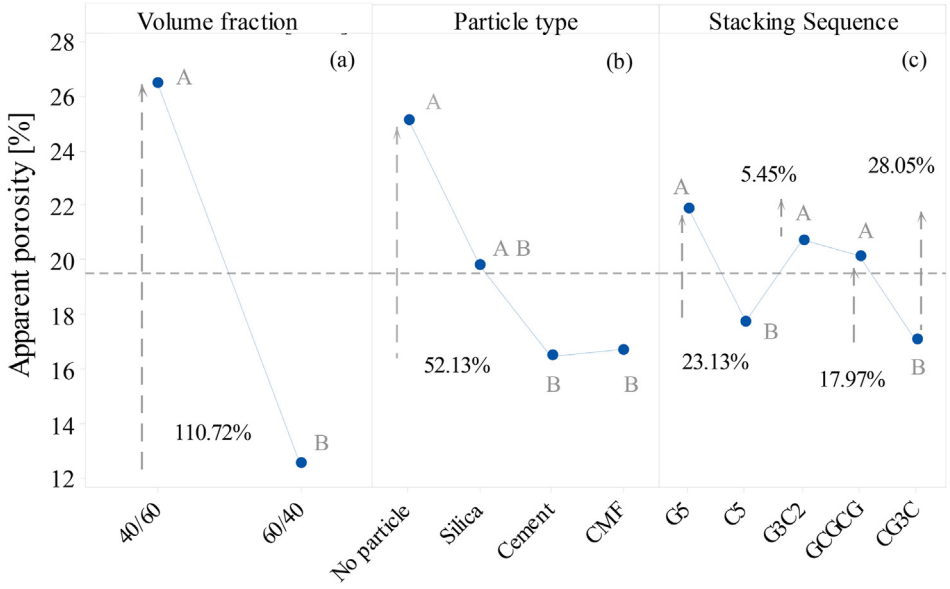

Fig. 4. Main effect plots for the mean apparent porosity [%].

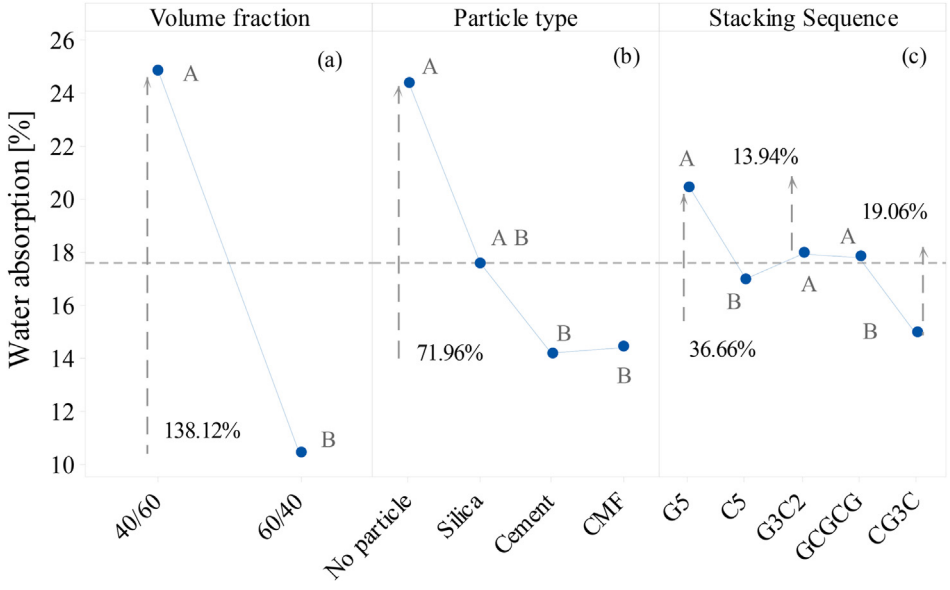

Fig. 5. Main effect plots for the mean water absorption [%].

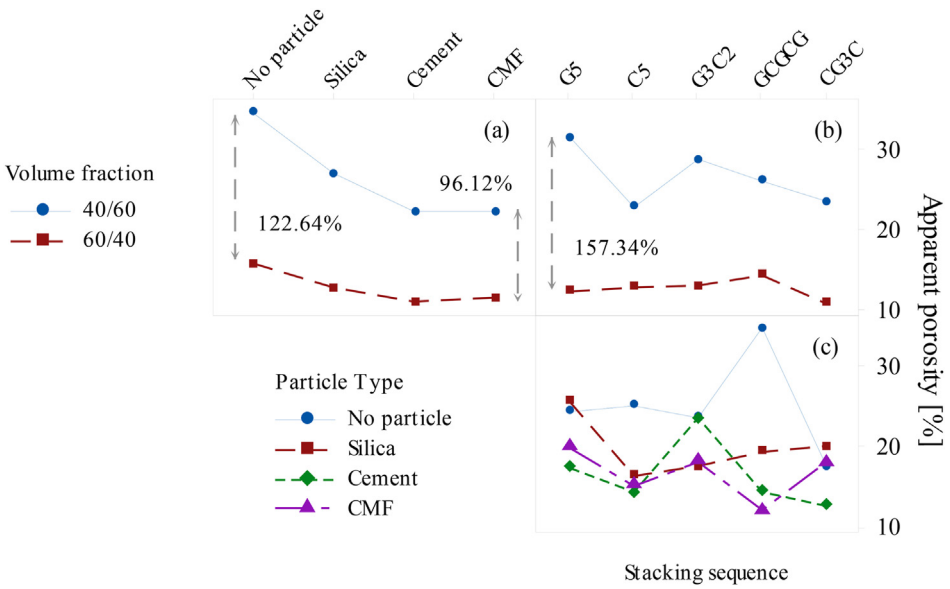

Fig. 6. Third-order interaction effect plots for the mean apparent porosity.

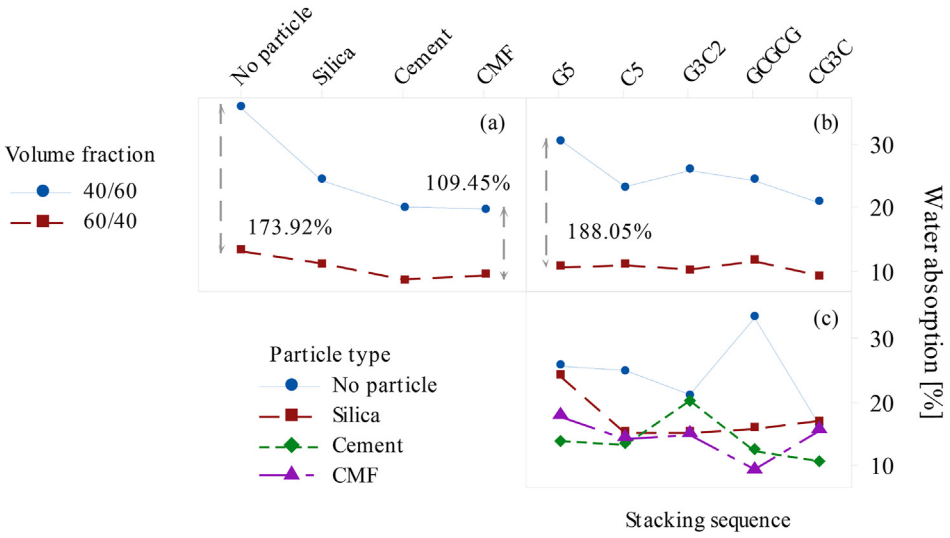

Fig. 7. Third-order interaction effect plots for the mean water absorption.

2.6. Scanning electron microscope analysis

The fibre/matrix interface and the distribution of dispersive phases within the hybrid laminates are examined using a scanning electron microscope, Hitachi TM 3000 model. The accelerating voltage is set at 15 kV. SEM analyses are performed only on carbon fibre samples (C_5) due to their minimal image interference and better electron conductivity [28].

3. Results

3.1. Physical properties

Table 3 shows the ANOVA results related to physical responses. All main factors and interactions are significant for apparent density, apparent porosity and water absorption (P-value $\leq$ 0.05). The matrix/fibre volume fraction is the design factor that most affects the apparent porosity and water absorption, with a contribution of 54.96% and 51.46%, respectively. It is also evident that the factor that makes the main contribution to apparent density is the fibre stacking sequence. The Anderson-Darling normality test for residuals generated by porosity, water absorption and apparent density responses reach P-values of 0.296, 0.102 and 0.261 (>0.05), respectively [26]. Therefore, the distribution of residues of physical variables showed normal behaviour. Figs. 3–10 present the results of the grouping treatment obtained by Tukey's multiple comparison tests, in which statistically equivalent means are represented by equal letters [26].

Apparent porosity and water absorption data range from 8.75% to 28.09% and 7.42%–26.15%, respectively. The P-values and the significant interactions are the same for both physical responses, showing a mutual dependence, since the apparent porosity also contributes to the water absorption capacity. Figs. 4a and 5a show that higher amounts of matrix phase (60/40) contribute to reducing porosity and water absorption, with percentages increasing between 110.72% and 138.12%, respectively. This behaviour can be attributed to the greater wettability of the fibres, when more matrix phase is mixed, which leads to a reduction of pores and internal voids and, therefore, to water percolation.

Figs. 6 and 7 show the third-order interaction effect plots for the mean

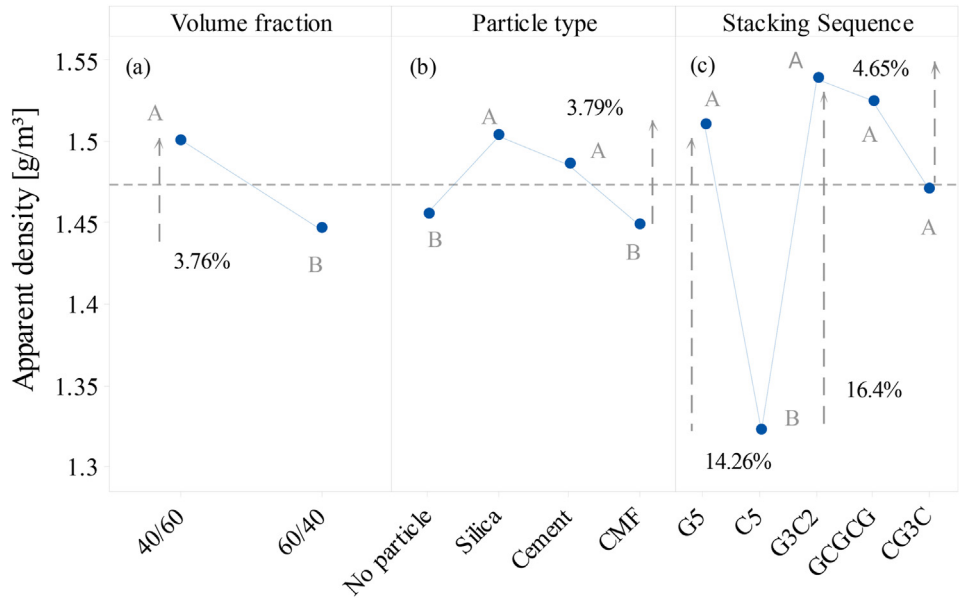

Fig. 8. Main effect plots for the mean apparent density.

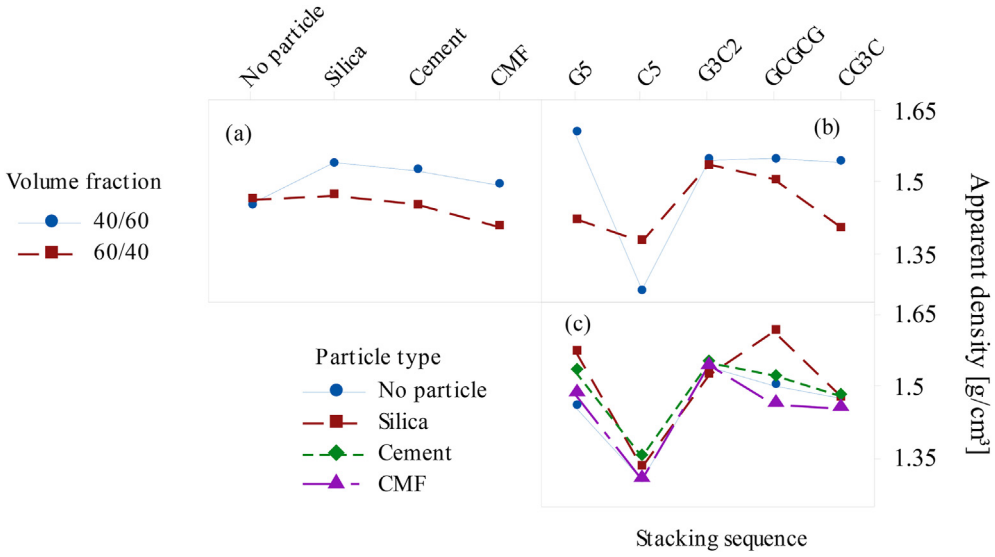

Fig. 9. Third-order interaction effect plots for the mean apparent density.

apparent porosity and water absorption responses, respectively. The lowest porosity is achieved by a hybrid system composed of carbon microfibres (CMF) and carbon layers, as shown in Fig. 4a and b - 5a,b. In general, the incorporation of particles reduces porosity, which is related to the reduction of microvoids at the interface. Hsu and Kevin [29] reported that the pores in the composite system tend to occur mainly at the ply interfaces and are elongated towards the adjacent fibres. Therefore, the smaller particle size from CMFs (Fig. 2c) contributes to better packing and rheology of the system.

The water absorption of the G_5 glass composition increases by approximately 36.66% over the C_5 carbon composition. At the same glass/carbon fibre ratio, the water absorption percentage of the G_3C architecture decreases by nearly 13.94%, while the water absorption of the CG_3C composite decreases by 33%, as shown in Fig. 5c. This behaviour can be attributed to the partially hydrophobic characteristics of the carbon fibre in the composite. Commercial CFs, in general, are hydrophobic due to the high temperature of the manufacturing process [30] and can be more wettable, depending on the number of oxygen moieties present on the surface [31,32]. As a result, the internal hybrid composite structure exhibits mixed wettability, with different hydrophilic (glass fibres) and partially hydrophobic (carbon fibres) fractions. Therefore, the contribution of carbon fibre in reducing the water absorption of the composite is substantially significant due to its hydrophobic characteristics and inert chemical properties when compared to glass fibre, mainly on the upper and lower sides [33].

The apparent density values range from 1.22 to 1.79 g/cm^3. The ANOVA results (Table 3) reveal that the fibre stacking sequence is the main factor affecting density (50.47% contribution), followed by the interaction “fibre/matrix volume fraction*stacking sequence” (20.12%). The glass fibres in the hybrid stacking sequence lead to an increase in bulk density. The higher density is evidenced by a hybrid system composed of carbon-glass fibres, especially G_3C_2 configuration and a lower matrix phase (40/60) (Fig. 8a–c). Stacks G_3C_2, GCGCG and CGGGC have similar density values, as shown by the same letter group-A (Fig. 8c). The fibre reinforcements may be responsible for the slight increase in the composite density, since the epoxy polymer (~1.16 g/cm^3 -

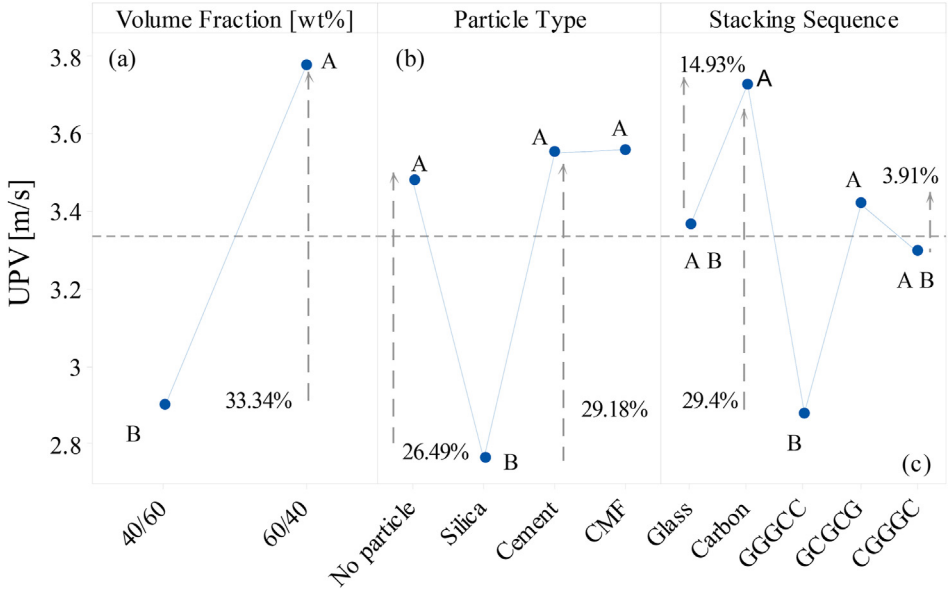

Fig. 10. Main effect plot for the mean UPV.

Melo et al. [34]) is less dense than the other fibre components. Glass fibres (~2.65 g/cm^3 - Detomi et al. [35]) possess a higher density when compared to carbon fibres (~1.77 g/cm^3 - Santos et al., [36]), increasing the apparent density of hybrid laminates. Note that a greater amount of matrix phase (60/40) provides not only less density (Fig. 8a) but also less porosity (Fig. 4a).

Notably, the particle type induces different behaviours that depend on the fibre-stacking sequence (Fig. 8). The presence of rigid particles in the system causes a slight increase in the apparent density (Fig. 8b), in which the density values of the hybrid particle system are higher than the reference condition due to the higher particle density: cement (~2.8 g/cm^3 [37]), silica (~2.7 g/cm^3 [38]) and CMF (~1.7 g/cm^3 [39]). However, cement and silica systems have similar densities, as shown by the same group letter (A) in Fig. 8b. Likewise, the CMF system has similar apparent densities to the reference condition (without particle), as shown by letter group B (Fig. 7b).

Fig. 9 shows the interaction effect plot for the mean apparent density. The interactions between the factors, stacking sequence and volume fraction (Fig. 9b) and stacking sequence and particle type (Fig. 9c) are evident. The system is too complex to assign an explanation for each configuration; however, the main change is related to the volume (thickness) of the samples as a function of the stacking sequence, presenting a greater contribution (see Table 3), consequently affecting the density of the composites.

3.2. Ultrasonic pulse velocity

Ultrasonic pulse velocity (UPV) is determined by the vibrational and rotational energy of intra- and inter-molecular interactions. Ultrasonic vibrational waves in hybrid fibre-reinforced composites are mainly related to the absorption of amorphous epoxy polymer and the scattering of fibres and particles [1,2]. The wave propagates faster in a continuous solid; i.e., a higher porosity level tends to reduce the UPV. It is noteworthy that the porosity results of the composites, shown in the previous section (3.1), follow the behaviour of the UPV.

Pulse velocity data ranges from 1.69 to 5.8 m/s. A full factorial design of $2^1 4^1 5^1$ is considered for this response. The underlined P-values in Table 4 indicate the significant factors and/or interactions that affect the UPV. Anderson Darling's normality test validates the analysis, showing a P-value (0.290) greater than 0.05. A higher R^2 reveals that the statistical model presents good predictability for the data.

Table 4
ANOVA results for pulse velocity.

Main factor and interactions	Full factorial design $2^1 4^1 5^1 = 40$	
	UPV [ms^{-1}]	
	Contribution	P-value ≤ 0.05
Volume Fraction	28.69%	0.000
Particle Type	13.15%	0.000
Stacking Sequence	9.72%	0.000
Fraction*Particle type	2.65%	0.000
Fraction*Stacking	6.58%	0.000
Particle type*Stacking	16.54%	0.000
Fraction*Particle Type*Stacking	20.76%	0.000
R^2 (adj)	96.24%	
Anderson-Darling test	P-value = 0.290 $\geq$ 0.05	

Figs. 10 and 11 show the main and interaction effect plots, respectively, for the mean UPV. The percentage contribution shown in Table 4 reveals that the UPV is most affected by the volume fraction factor (28.69%), followed by the third-order interaction effect (20.76%). The UPV increases by 33.34% at a high matrix/fibre ratio (60/40), as shown in Fig. 10a, which also led to a reduced porosity level (Fig. 4a). According to Sokolovskaya et al. [18] and Chang et al. [17], the increase in pores contributes to the delay in wave propagation. Thus, a higher matrix phase content also reduces the void volume, increasing the dispersion of the ultrasonic pulse waves.

In general, incorporating inert silica particles reduces the UPV (Fig. 10b), which is attributed to more voids at its interface. Silica-reinforced composites achieve higher porosity than cement and CMF reinforcements, as shown in Fig. 4b. On the other hand, cement particles increase the UPV, which can be attributed to the possible chemical interaction with the epoxy polymer [21,40]. This particular feature can affect the UPV results, since a denser solid gives higher UPV values [21]. The aspect ratio of the CMFs and their small size also contribute to better packing of the system, reducing voids (Fig. 3b) and increasing UPV. Trtnik et al. [7] reported that the size, type, shape and amount of the aggregate greatly influence the strength-velocity relationship. The aggregate cannot be neglected to predict physical and mechanical responses accurately.

Unlike glass fibre composites, carbon fibre composites led to reduced porosity (Fig. 4c) and increased UPV, as shown in Fig. 10c. Carbon fibre

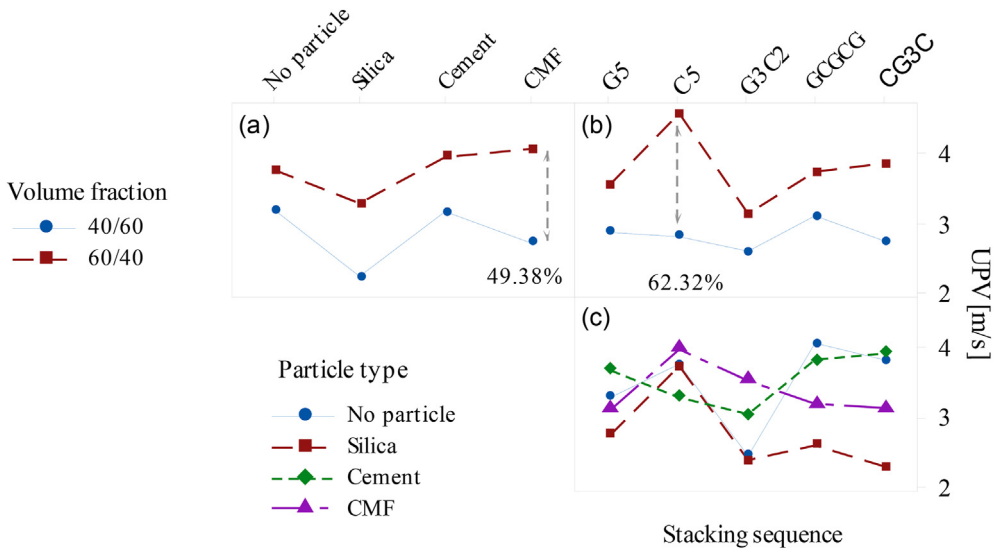

Fig. 11. Third-order interaction effect plot for the mean UPV.

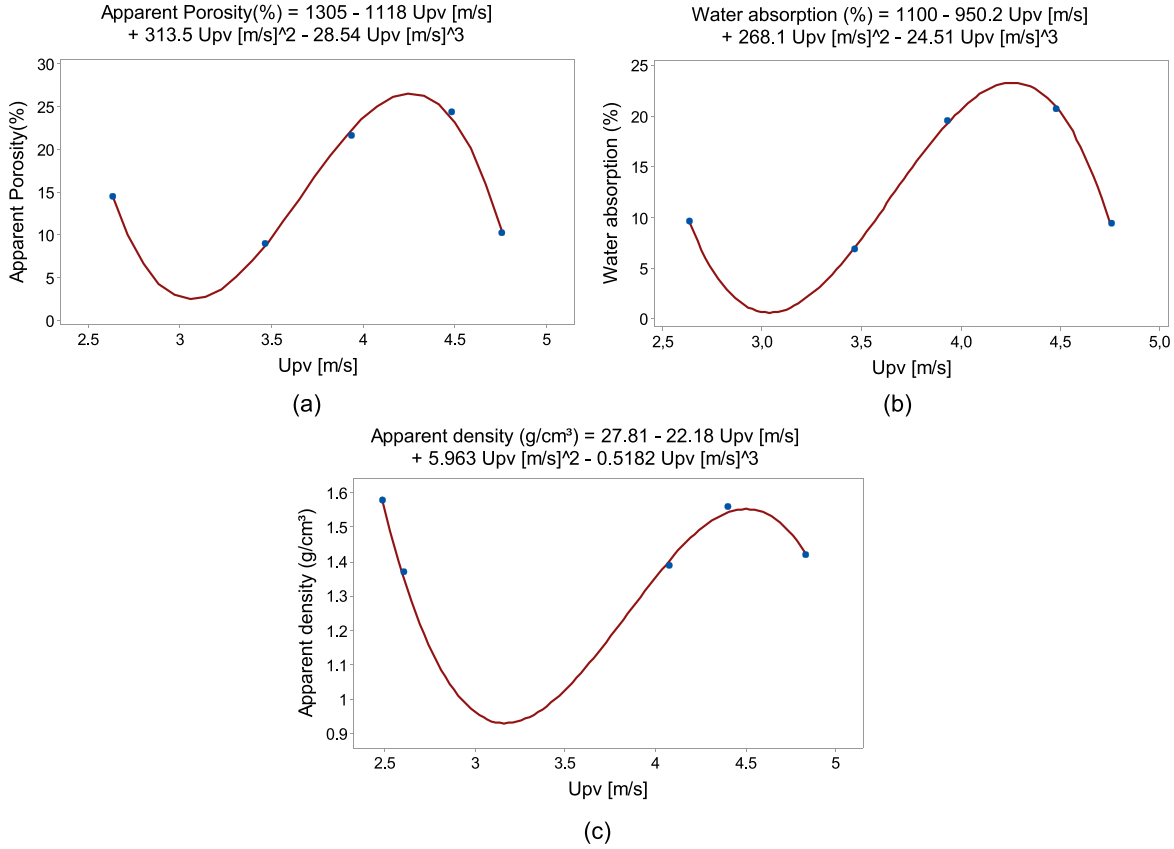

Fig. 12. Relations between UPV values and physical properties – (a) apparent porosity, (b) water absorption and, (c) apparent density.

composites and CMF factor levels provide higher UPV values, especially at the 60/40 level (Fig. 12a and b), which is attributed to the superior wettability of carbon fibres compared to glass fibres, resulting in a denser material. Silica and CMFs exhibit good interaction with carbon fibre composites, revealing increases in UPV, as shown in Fig. 10c. Cement particles achieve greater UPV when embedded in glass fibre composites and hybrid laminates, especially for GCGCG and CGGGC configurations. In addition, the UPV values of the laminates without particles (Fig. 11c) also indicate that it is better to alternately combine glass and carbon fibres (GCGCG) than to stack them jointly as GGGCC or CGGGC.

3.3. Correlations between physical properties and UPV

Correlation analyses are performed to model the relations between physical properties and UPV. Tables 5–7 show the equations and adjustments of the correlation models. The validity and adequacy of the relations are verified by the coefficient of determination (R^2) and standard error (Std). The std is the standard deviation or error term,

Table 5
Correlations between apparent porosity and UPV.

Fraction	Particle	Regression equation	R^2 (adj)	Std
40/60	No particle	Ap(%) = 185 - 67UPV - 12.4 UPV^2 + 5.58UPV^3	93.7%	4.229
60/40		Ap(%) = 1305 - 1118UPV + 313.5UPV^2 - 8.54UPV^3	99.6%	0.816
40/60	Silica	Ap(%) = 24.64–31.00UPV + 13.71UPV^2 – 1.996 UPV^3	98.9%	0.042
60/40		Ap(%) = - 1235 + 1114UPV - 324.2 UPV^2 + 30.78UPV^3	95.9%	1.063
40/60	Cement	Ap(%) = - 7.47 + 7.69UPV - 2.164UPV^2 + 0.2019UPV^3	83.0%	0.098
60/40		Ap(%) = −1516 + 1164UPV - 293.6UPV^2 + 24.52UPV^3	81.7%	1.011
40/60	CMF	Ap(%) = - 25.55 + 30.70UPV - 11.39UPV^2 + 1.384UPV^3	79.5%	0.117
60/40		Ap(%) = - 339.2 + 256.3UPV - 60.69 UPV^2 + 4.635UPV^3	95.6%	0.581

Table 6
Correlations between water absorption and UPV.

Fraction	Particle	Regression equation	R^2 (adj)	Std
40/60	No particle	Wt (%) = 41.4 + 91.0UPV - 70.0UPV^2 + 12.56UPV^3	98.8%	1.424
60/40		Wt (%) = 1100–950.2UPV + 268.1UPV^2 – 24.51UPV^3	99.7%	0.372
40/60	Silica	Wt (%) = 4318 - 6007UPV + 2742UPV^2 - 406.2UPV^3	77.6%	4.925
60/40		Wt (%) = - 1475 + 1333UPV - 389.8UPV^2 + 37.16UPV^3	97.7%	0.851
40/60	Cement	Wt (%) = 1654 - 1506UPV + 453.7UPV^2 - 44.73UPV^3	89.4%	4.469
60/40		Wt (%) = - 2755 + 2013UPV - 483.6UPV^2 + 38.26 UPV^3	83.4%	1.033
40/60	CMF	Wt (%) = - 1176 + 1427UPV −555.2UPV^2 + 70.38UPV^3	99.1%	1.714
60/40		Wt (%) = - 202.0 + 158.0UPV - 38.10UPV^2 + 2.950UPV^3	94.3%	0.472

Table 7
Correlations between apparent density and UPV.

Fraction	Particle	Regression equation	R^2 (adj)	Std
40/60	No particle	ρ (g/cm^3) = - 68.00 + 73.45UPV - 25.47UPV^2 + 2.9UPV^3	93.6%	0.038
60/40		ρ (g/cm^3) = 27.81–22.18UPV + 5.963UPV^2 - 0.5182UPV^3	98.4%	0.025
40/60	Silica	ρ (g/cm^3) = 66.39–87.22UPV + 38.36UPV^2 - 5.482UPV^3	99.1%	0.019
60/40		ρ (g/cm^3) = - 24.11 + 23.03UPV - 6.729 UPV^2 + 0.6388UPV^3	95.5%	0.029
40/60	Cement	ρ (g/cm^3) = 16.06–14.60UPV + 4.728UPV^2 - 0.4926UPV^3	79.7%	0.121
60/40		ρ (g/cm^3) = - 46.98 + 36.31UPV - 8.946UPV^2 + 0.7232UPV^3	93.7%	0.032
40/60	CMF	ρ (g/cm^3) = - 28.82 + 34.23UPV - 12.66 UPV^2 + 1.536UPV^3	99.7%	0.016
60/40		ρ (g/cm^3) = - 22.24 + 17.41UPV - 4.160UPV^2 + 0.3206UPV^3	85.9%	0.048

calculated by the square root of the mean square residue. The R^2 coefficient indicates how well the variability of observed physical responses can be explained or predicted by the independent variables. Higher values of R^2 correspond to a more robust model between independent and dependent responses. The R^2 range from 77.6% to 99.1%, indicating proper correlations between physical properties and UPV.

The relationships between the responses are shown in Fig. 12. An indication of the cubic relationship is identified among the pulse wave values and the apparent porosity (Fig. 12a), water absorption (Fig. 12b) and density (Fig. 12c). The physical properties vs UPV present an exponential trend within the range of this experimental design. It is worth mentioning that all the considered factors significantly affect the UPV response (p-value ≤ 0.05, Table 4).

This information is valuable and innovative in composites technology since the models can be employed to predict and estimate physical properties based on the UPV data and identify defects and damages of hybrid composites.

Fig. 13 shows the backscattered electron images (15 kV) of the C_5 (carbon) samples at × 500 and × 1000 magnification. The silica particles are randomly-dispersed, revealing some penetrations into the carbon fabric. This characteristic contributes to the greater porosity of the hybrid system. Furthermore, the UPV values decrease with silica inclusions (Fig. 10b), which is attributed to the fact that a certain amount of energy from the ultrasonic wave is lost through a porous structure. Ashorth et al. [41] reported that the modal responses largely depend on the composition and manufacture of the composites, i.e. greater porosity increases the scattering and dispersion of the energy waves. In addition, due to the viscoelastic behaviour, a higher amount of epoxy matrix tends to increase the modal response, as shown in Fig. 10a.

Fig. 13b shows the carbon layers containing cement particles. The fibres are not evident, demonstrating a good dispersion of the particles in the matrix phase. Different levels of grayscale reveal the presence of a heterogeneous microstructure, typical in the hydration of Portland cement. The brighter area in backscattered images displays denser regions, which indicates the presence of hydrated products. Some researchers [21,39] have pointed out the evidence of chemical interaction between Portland cement and epoxides with the formation of hydrated calcium silicates (CSH - $Ca_2SiO_4.H_2O$) and calcium hydroxide (Portlandite - $Ca(OH)_2$ (s)), which make the particles well compacted. As a result, particles can spread and become more homogeneous in the system, resulting in better wave scattering. A higher damping factor obtained by cement-reinforced composites (Fig. 10b) indicates a chemical interaction between the matrix and the particle. Javanmardy et al. [42] found a tangible physical relation between modal changes and stiffness in a composite system. Despite the complexity of the system, it is noted that the insertion of cement can be an excellent option to enhance the UPV characteristics of carbon fibre-reinforced composites.

In contrast, carbon microfibres (CMF) characteristics, such as shape and size, can act as barriers against crack propagation [43]. The high geometric aspect ratio of the CMF in the interlaminar region may be responsible for enhancing the stress distribution of the composite, contributing to an increase in its damping capacity. The average cylindrical size in the cross-section is significantly smaller (between 15 and 40 μm), and these fibres have a less dense surface. CMFs have a higher aspect ratio and are, therefore, less affected due to the presence of epoxy polymer on the fibre surfaces, which contributes to adhesive compatibility and wave dispersion.

4. Conclusion

This paper identifies the effect of different micro-macro reinforcements on the ultrasonic pulse velocity and physical responses of a hybrid fibrous-particulate system. In particular, correlation analyses of water absorption, apparent porosity and density against UPV are performed. The surface and dispersion of the evaluated particles primarily affect the physical properties. The apparent porosity and water absorption of the FRCs are reduced by 110.72% and 138.12%, respectively, especially when using a greater amount of polymeric matrix. Cement/CMF particles and the CG3C configuration induce further porosity reductions. Apparent density is significantly affected by fibre arrangement. The highest density is achieved by glass fibre laminates (G5) without particles and a lower amount of epoxy-matrix (40%). In general, the physical responses are mainly influenced by the surface area and

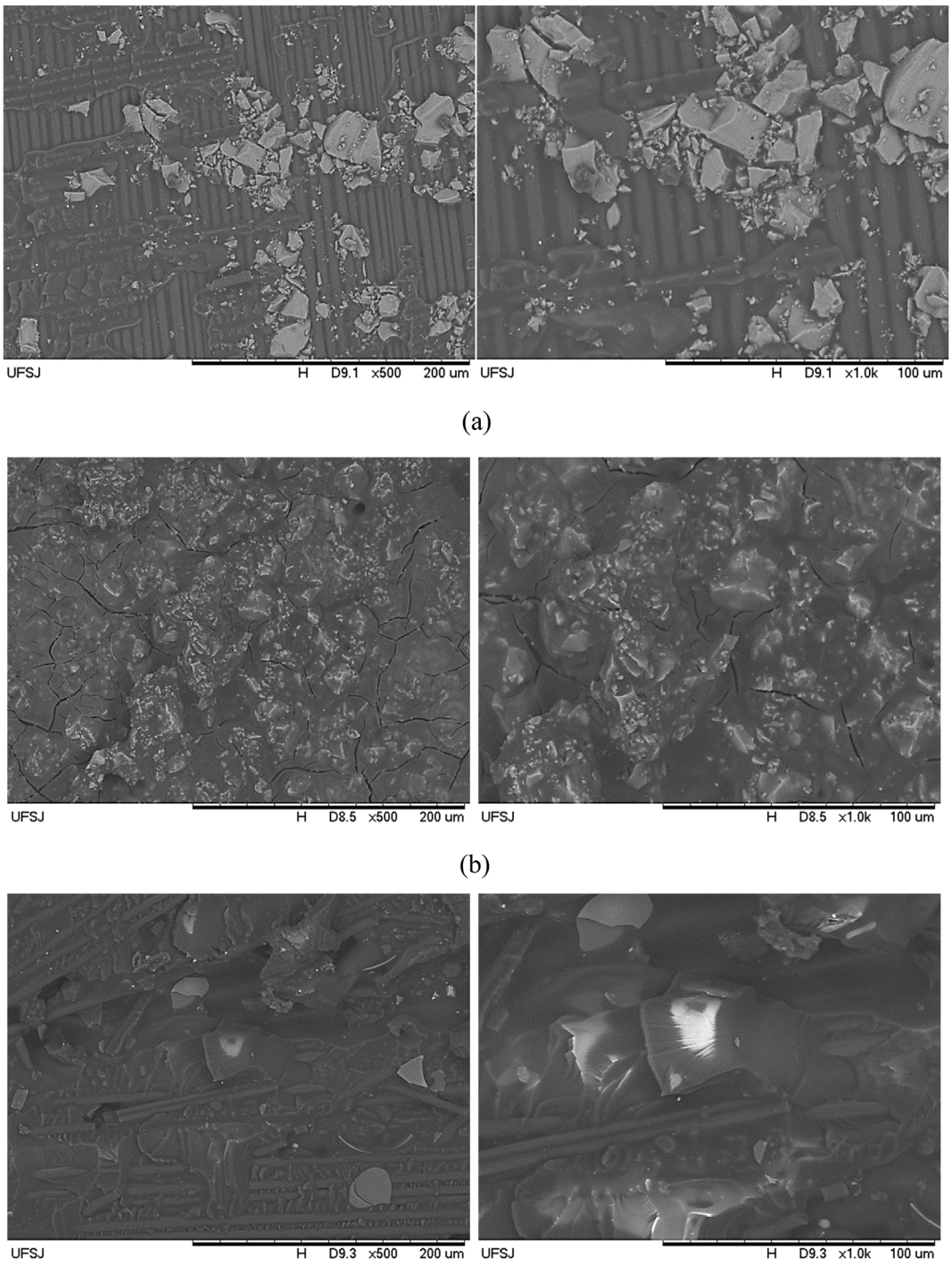

Fig. 13. SEM images of the surfaces of C5 sample with (a) Silica, (b) Cement and (c) CMF at 60/40 vol fraction.

dispersion of the particles. Laminates composed of the lowest amount of matrix phase lead to an increase in density (4.49%) and a reduction in porosity (110.72%). The UPV response is substantially affected by the third-order interaction effect. Peak values are obtained for composites made from carbon fibres, higher amounts of matrix phase, carbon fibres and CMF wastes. The results of water absorption, apparent porosity and density showed an intrinsic relationship with the pulse velocity measurements providing exponential models capable of estimating these physical properties. Further investigations on the quantitative assessment of the UPV incorporating defects or damages in the hybrid system will be carried out considering numerical and analytical models combined with the technique of artificial neural networks.

Data availability

The raw/processed data required to reproduce these findings cannot be shared at this time as the data also forms part of an ongoing study.

Declaration of competing interest

The authors declare that there is no conflict of interest.

Acknowledgements

The authors acknowledge the Brazilian Research Agencies, CAPES (MSc scholarship), CNPq (PQ-309885/2019–1) and FAPEMIG (PPM-00075-17) for the financial support provided.

References

[1] V. Marcantonio, D. Monarca, A. Colantoni, M. Cecchini, Ultrasonic waves for materials evaluation in fatigue, thermal and corrosion damage: a review, Mech. Syst. Signal Process. 120 (2019) 32–42, https://doi.org/10.1016/j.ymssp.2018.10.012.

[2] C. Vipulanandan, V. Garas, Electrical resistivity, pulse velocity and compressive properties of carbon fiber reinforced cement mortar, J. mater. Civ. Eng. (2008) 93–101.

[3] G. Karaiskos, A. Deraemaeker, D.G. Aggelis, D.V. Hemelrijck, Monitoring of concrete structures using the ultrasonic pulse velocity method, Smart Mater. Struct. 24 (11) (2015), 113001, https://doi.org/10.1088/0964-1726/24/11/113001.

[4] T.H. Panzera, J.C. Rubio, C.R. Bowen, W.L. Vasconcelos, K. Strecker, Correlation between structure and pulse velocity of cementitious composites, Adv. Cement Res. 20 (3) (2008) 101–108, https://doi.org/10.1680/adcr.2008.20.3.101.

[5] K. Nascimento, A. Santos, A. Vale, T. Panzera, C. E. S. da Silva, and P. H. R. Borges, "Correlations on pulse velocity and physic-mechanical properties of impact-compacted cement mortar containing quartz and recycled PP aggregates," J. Test. Eval. 48 (2023).

[6] Y. Lin, C.P. Lai, T. Yen, Prediction of ultrasonic pulse velocity in concrete, ACI Mater. J. 100 (1) (2003) 21–28.

[7] G. Trtnik, F. Kavcic, G. Turk, Prediction of Concrete Strength Using Ultrasonic Pulse Velocity and Artificial Neural Networks Ultrasonics, vol. 49, 2009, pp. 53–60.

[8] J. Zhang, L. Qin, Z. Li, Hydration monitoring of cement-based materials with resistivity and ultrasonic methods, Mater. Struct. 42 (2009) 15–24.

[9] G. Trtnik, G. Turk, F. Kavèiè, V.B. Bosiljkov, Possibilities of using the ultrasonic wave transmission method to estimate initial setting time of cement paste, Cement Concr. Res. 38 (2008) 1336–1342.

[10] G. Ye, K. van Breugel, A.L.A. Fraaij, Experimental study on ultrasonic pulse velocity evaluation of the microstructure of cementitious material at early age, Heron 46 (3) (2001) 161–167.

[11] M.F. Markham, Measurement of the elastic constants of fibre composites by ultrasonics, Composites 1 (2) (1969) 145–149, https://doi.org/10.1016/0010-4361(69)90059-7.

[12] S. Baste, R. El Guerjouma, B. Audoin, Effect of microcracking on the macroscopic behaviour of ceramic matrix composites: ultrasonic evaluation of anisotropic damage, Mech. Compos. Mater. 14 (1992) 15–31, https://doi.org/10.1016/0167-6636(92)90015-6.

[13] R. Böhm, W. Hufenbach, Experimentally based strategy for damage analysis of textile-reinforced composites under static loading, Compos. Sci. Technol. 70 (9) (2010) 1330–1337, https://doi.org/10.1016/j.compscitech.2010.04.

[14] B. Audoin, S. Baste, Ultrasonic evaluation of stiffness tensor changes and associated anisotropic damage in a ceramic matrix composite, J. Appl. Mech. 61 (2) (1994) 309, https://doi.org/10.1115/1.2901446.

[15] W. Hufenbach, R. Böhm, A. Langkamp, L. Kroll, T. Ritschel, Ultrasonic evaluation of anisotropic damage in multiaxially textile-reinforced thermoplastic composites made from hybrid yarns, Mech. Compos. Mater. 42 (2) (2006) 151–162, https://doi.org/10.1007/s11029-006-0026-3.

[16] A. Castellano, P. Foti, A. Fraddosio, S. Marzano, M.D. Piccioni, Mechanical characterisation of CFRP composites by ultrasonic immersion tests: experimental and numerical approaches, Compos. B Eng. 66 (2014) 299–310, https://doi.org/10.1016/j.compositesb.2014.04.024.

[17] J. Chang, C. Zheng, Q.-Q. Ni, The ultrasonic wave propagation in composite material and its characteristic evaluation, Compos. Struct. 75 (1–4) (2006) 451–456, https://doi.org/10.1016/j.compstruct.2006.04.040.

[18] Y.G. Sokolovskaya, N.B. Podymova, A.A. Karabutov, Verification of the Kramers-Kronig relations between ultrasonic attenuation and phase velocity in a finite spectral range for CFRP composites, Ultrasonics (2019), https://doi.org/10.1016/j.ultras.2019.03.004.

[19] A.-M. Zelenyak, N. Schorer, M.G.R. Sause, Modeling of ultrasonic wave propagation in composite laminates with realistic discontinuity representation, Ultrasonics 83 (2018) 103–113, https://doi.org/10.1016/j.ultras.2017.06.014.

[20] S.L.M. Ribeiro Filho, P.R. Oliveira, L.M.G. Vieira, T.H. Panzera, R.T.S. Freire, F. Scarpa, Hybrid bio-composites reinforced with sisal-glass fibres and Portland cement particles: a statistical approach, Compos. B Eng. 149 (2018) 58–65, https://doi.org/10.1016/j.compositesb.2018.05.019.

[21] T.H. Panzera, A.L.R. Sabariz, K. Strecker, P.H.R. Borges, D.C.L. Vasconcelos, W.L. Wasconcelos, Propriedades mecânicas de materiais compósitos à base de cimento Portland e resina epoxi, Cerâmica 56 (337) (2010) 77–82, https://doi.org/10.1590/s0366-69132010000100013.

[22] American Society for Testing and Materials, ASTM D792-13 (2013), Standard Test Methods for Density and Specific Gravity (Relative Density) of Plastics by Displacement, ASTM International, West Conshohocken, PA, 2013, https://doi.org/10.1520/D0792.

[23] American Society for Testing and Materials C1039-85 (2015), Standard Test Methods for Apparent Porosity, Apparent Specific Gravity, and Bulk Density of Graphite Electrodes, ASTM International, West Conshohocken, PA, 2015.

[24] American Society for Testing and Materials, ASTM D790-15e1 (2015), Standard Test Methods for Flexural Properties of Unreinforced and Reinforced Plastics and Electrical Insulating Materials, ASTM International, West Conshohocken, PA, 2015, https://doi.org/10.1520/D0790-15E01.

[25] British Standards Institution BSI, "BS 1881: Part 203: 1986: Measurement of Velocity of Ultrasonic Pulses in Concrete, 1986.

[26] D.C. Montgomery, Design and Analysis of Experiments, 6ª edition, John Wiley & Sons, Inc., Arizona, 2005.

[27] C.F.J. Wu, M. Hamada, Experiments: Planning, Analysis, and Parameter Design Optimisation, John Wiley & Sons, New York, 2000.

[28] R. Heu, S. Shahbazmohamadi, J. Yorston, P. Capeder, Target material selection for sputter coating of SEM samples, Microsc. Today 27 (4) (2019) 32–36.

[29] D.K. Hsu, H. Jeong, Ultrasonic velocity change and dispersion due to porosity in composite laminates, Rev. Prog. Quant. Nondestr. Eval. (1989) 1567–1573, https://doi.org/10.1007/978-1-4613-0817-1_197.

[30] S.J. Park, M.K. Seo, Germany, Carbon Fiber-Reinforced Polymer Composites: Preparation, Properties, and Applications, in Polymer Composites, vol. 1, Wiley-VCH Verlag GmbH & Co. KGaA, Weinheim, 2012.

[31] Y. Luo, Y. Zhao, Y. Duan, S. Du, Surface and wettability property analysis of CCF300 carbon fibers with different sizing or without sizing, Mater. Des. 32 (2) (2011) 941–946, https://doi.org/10.1016/j.matdes.2010.08.004.

[32] B.-H. Kim, D.H. Lee, K.S. Yang, B.-C. Lee, Y.A. Kim, M. Endo, Electron beam irradiation-enhanced wettability of carbon fibers, ACS Appl. Mater. Interfaces 3 (2) (2010) 119–123, https://doi.org/10.1021/am101064s.

[33] Dan-mallam Yakubu, T.W. Hong, M.S. Abdul Majid, Mechanical characterisation and water absorption behaviour of interwoven kenaf/PET fibre reinforced epoxy hybrid composite, Int. J. Polym. Sci. (2015) 1–13, https://doi.org/10.1155/2015/371958, 2015.

[34] A.B.L. Melo, L.F.L. Paiva, J.C. Santos, T.H. Panzera, R.T.S. Freire, A Statistical analysis of Epoxy polymer reinforced with micro ceramic particles, J. Res. Updates Polym. Sci. 5 (2016) 108–113.

[35] A.C. Detomi, R. M. dos Santos, S.L.M.R. Filho, C.C. Martuscelli, T.H. Panzera, F. Scarpa, Statistical effects of using ceramic particles in glass fibre reinforced composites, Mater. Des. 55 (2014) 463–470, https://doi.org/10.1016/j.matdes.2013.09.026.

[36] J.C. Santos, L.M. Vieira, T.H. Panzera, A.L. Christoforo, M.A. Schiavon, F. Scarpa, Hybrid silica micro and PDDA/nanoparticles-reinforced carbon fibre composites, J. Compos. Mater. 51 (6) (2016) 783–795, https://doi.org/10.1177/0021998316655392.

[37] P. Lessing, High-density and radiation-shielding concrete, Dev. Formul. Reinforcement Concr. (2008) 44–78.

[38] J. Campbell, Moulding. Complete Casting Handbook, 2015, pp. 797–819, https://doi.org/10.1016/b978-0-444-63509-9.00015-7.

[39] C. Thomas, P.H.R. Borges, T.H. Panzera, A. Cimentada, I. Lombillo, Epoxy composites containing CFRP powder wastes, Compos. B Eng. 59 (2013) 260–268.

[40] C.C. Martuscelli, J. Cesar dos Santos, P. Resende Oliveira, T. Hallak Panzera, M.T. Paulino Aguilar, C. Thomas Garcia, Polymer-cementitious composites containing recycled rubber particles, Construct. Build. Mater. 170 (2018) 446–454, https://doi.org/10.1016/j.conbuildmat.2018.03.017.

[41] S. Ashworth, J. Rongong, P. Wilson, J. Meredith, Mechanical and damping properties of resin transfer moulded jute-carbon hybrid composites, Compos. B Eng. 105 (2016) 60–66, https://doi.org/10.1016/j.compositesb.2016.08.019.

[42] A. Javanmardi, R. Abadi, A.K. Marsono, M. Md Tap, Z. Ibrahim, A. Ahmad, Correlation of stiffness and natural frequency of precast frame system, Appl. Mech. Mater. 735 (2015) 141–144. 10.4028/www.scientific.net/am.

[43] S.L.M. Ribeiro Filho, C. Thomas, M.V. Donadon, F. Scarpa, T.H. Panzera, The impact of hybrid fibre-particle composited based on a full factorial design, Mater. Today Commun. 31 (2022), https://doi.org/10.1016/j.mtcomm.2022.103459.